PASJ: Publ. Astron. Soc. Japan **48**, 639–655 (1996)

Intergalactic Absorption Due to Extended Gaseous Clouds at High Redshifts

Kiyomi DENDA
Institute of Astronomy, Faculty of Science, The University of Tokyo, 2-21-1 Osawa, Mitaka, Tokyo 181
E-mail(KD): denda@mtk.ioa.s.u-tokyo.ac.jp
and
Satoru IKEUCHI
Department of Earth and Space Science, Faculty of Science, Osaka University, Toyonaka, Osaka 560

(Received 1996 March 1; accepted 1996 July 19)

Abstract

In order to examine the line-blanketing effect due to gaseous clouds at high redshifts, we have calculated the ionization states of gas clouds of subgalactic mass scale exposed to a UV radiation field that can reproduce the ionization states of the Lyman limit systems (LLSs) along the line of sight to quasar HS 1700 + 6416. We also adopted the integrated UV radiation from the observed quasars modified by the intervening absorption due to the Lyman α forest and LLSs as an ionizing spectrum. Our photoionization models can explain the observed H I column-density distribution, the observed C IV/H I ratio and the observed optical depths of H I and He II. We conclude that the integrated UV background models can well explain the ionization states of both the IGM and Lyman α clouds at $z \sim 2$–3. The gaseous mass of the Lyman α clouds follows a power-law form as $dn/dM_c \propto M_c^{-\delta}$ with $\delta \sim 2$–2.5 in the 10^8–$10^{11} M_\odot$ range. The majority of the dark baryon probably consists of the IGM.

Key words: Galaxies: intergalactic medium — Opacities — Quasars — Ultraviolet

1. Introduction

Recently, the high-resolution ($R \equiv \lambda/\Delta\lambda > 10^4$) spectra of quasars have been obtained with the echelle spectrograph (HIRES) on the Keck 10-m telescope, which have revealed a new picture of Lyman α clouds. First, Cowie et al. (1995) showed that roughly half of the Lyman α clouds at $\langle z \rangle \sim 2.6$ with $N_{\rm H\,I} \geq 3 \times 10^{14}{\rm cm}^{-2}$ have measurable C IV lines with $N_{\rm C\,IV} > 10^{12}{\rm cm}^{-2}$, and that the metallicity of such Lyman α clouds is $\sim 10^{-2}$ of the solar value. They analyzed the velocity structure of the corresponding C IV lines, and showed that the Lyman α clouds are complexes of cloudlets confined by a gravitational mechanism. Second, Songaila, Hu, and Cowie (1995) detected diffuse Lyman α clouds at $z \sim 3$ with low column densities of neutral hydrogen ($\sim 2 \times 10^{12}{\rm cm}^{-2}$) in their high-resolution spectrum of quasar Q0302 − 003. They then showed that the He II line blanketing due to the Lyman α clouds can explain the He II absorption feature at $z \simeq 3$ tentatively detected by Jakobsen et al. (1994). Third, Hu et al. (1995) have revealed that the observed column-density distribution of H I can be expressed as a single power-law form with $dn/dN_{\rm H\,I} \propto N_{\rm H\,I}^{-1.46}$ in the column density range of $2 \times 10^{12} \leq N_{\rm H\,I}({\rm cm}^{-2}) \leq 3 \times 10^{14}$. They analyzed the velocity distribution of the Lyman α clouds and discussed clouds' origin.

Since the spectral resolution is greatly improved, the spatial distribution of the Lyman α clouds shows some evidence of small-scale clustering, which may depend on their column density (Crotts 1989; Chernomordik 1995; Cristiani et al. 1995). Morris et al. (1993) reported that the Lyman α clouds along the line of sight to quasar 3C 273 are not distributed at random with respect to galaxies. However, the cloud–galaxy correlation is not as strong as the galaxy–galaxy correlation. Bahcall et al. (1996) also showed that the Lyman α clouds at low redshift may be closely associated with galaxies. Therefore, at least some populations of the Lyman α clouds are metal-enriched gas clouds, probably associated with high-redshift galaxies.

Jakobsen et al. (1994) have reported a tentative detection of the He II Gunn-Peterson optical depth at $z \sim 3$ with the Faint Object Camera (FOC) on the repaired Hubble Space Telescope (HST). The 90% confidence bound on the He II optical depth gives the lower limit as $\tau_{\rm He\,II} > 1.7$. Because this absorption feature on the line of sight to quasar Q0302−003 was detected at low spectral resolution, $\Delta\lambda \simeq 20$ Å , it is not clear whether this absorption is really due to He II in the IGM, i.e., the He II Gunn-Peterson optical depth. This feature could be interpreted either by He II line blanketing originating in

Lyman α forests, provided that there is a numerous population of weak Lyman α clouds with $N_{\rm H\,I} \lesssim 10^{12}{\rm cm}^{-2}$ (Jakobsen et al. 1994; Madau, Meiksin 1994). It is also possible that the reionization of He II in the IGM was not yet completed by $z \sim 3$ (Madau, Meiksin 1994). If the number of the He II ionizing photons emitted per second from the central source is much less than the H I ionizing photons, the He III region will trail behind the H II region. The remaining He II is possibly responsible for the observed He II absorption feature.

Recently, Songaila et al. (1995) reported diffuse Lyman α clouds with $N_{\rm H\,I} \sim 2 \times 10^{12}{\rm cm}^{-2}$, and showed that the He II line blanketing of the Lyman α clouds can explain the observed He II absorption feature at $z \simeq 3$. In their analysis, they followed the approximation described by Miralda-Escudé (1993), and estimated the effective optical depth of He II absorption arising from the Lyman α clouds as a function of both the optical-depth ratio at the center of the He II and H I lines, and the ratio of those Doppler parameters. Moreover, they derived the ratio of the ionizing intensity at the H I ionization edge to that at the He II edge, $S_{\rm L}$, by analyzing the ionization states of the metallic absorption systems along the line of sight to the quasar Q0200−330. They concluded that the He II absorption feature in the spectrum of Q0302−003 may be produced by a line-blanketing effect due to the Lyman α clouds.

Another observation required the modified picture of the UV background radiation. The Faint Object Spectrograph (FOS) on HST have revealed that the Lyman limit systems along the line of sight to quasar HS 1700 + 6416 (Reimers et al. 1992; Vogel, Reimers 1993, 1995; Reimers, Vogel 1993) have many ions at various ionization levels, simultaneously. The observed absorption properties are different from the predicted ionization states based on the canonical UV background models ($f_\nu \propto \nu^{-\alpha}$ with $\alpha \simeq 1$). Such a *standard* model fails to interpret new observations as the He II absorption feature at $z \sim 3$ reported by Jakobsen et al. (1994) and ionization states of the Lyman limit systems along the line of sight to quasar HS 1700 + 6416 (Madau, Meiksin 1994; Giroux et al. 1994). We then constructed more complicated photoionization models which can reproduce the ionization states of the metallic systems at $z \simeq 2$–3, especially observations of the Lyman limit systems (LLSs) along the line of sight to quasar HS 1700 + 6416 (Denda, Ikeuchi 1995, hereafter Paper I).

In this paper we examine the line-blanketing effect due to gaseous clouds at high redshifts. Previous studies (e.g., Miralda-Escudé 1993; Madau, Meiksin 1994) estimated the accumulated He II optical depth due to the Lyman α clouds using the observed H I column-density (or equivalent-width) distribution and the column-density ratio, $N_{\rm He\,II}/N_{\rm H\,I}$, derived from a simple photoionization model. On the other hand, we have calculated the ionization states of gas clouds of subgalactic mass scale exposed to a UV radiation field, which explains the observed ionization states of the LLSs on the line of sight to quasar HS 1700+6416. We then calculated the column-density distribution of H I, He I, and He II, and finally obtained the effective optical depths of these ions due to 'Lyman α clouds' at $z \simeq 3$. In section 2, we describe the photoionization model and show the resultant ionization states of the Lyman α clouds in section 3. The line-blanketing effect and the Gunn-Peterson optical depth are described in section 4. Section 5 gives the conclusions.

2. Photoionization Model

2.1. *Ionizing Background Radiation*

Our optimum model spectra have a suitable break at the He II ionization edge, and include the contribution of the soft X-ray radiation from quasars. In our study we adopted spectral models T15Mh, T07Mh, and T15Ll of Paper I and the integrated UV radiation from the observed quasars modified by the intervening absorption due to the Lyman α forest and LLSs (for details, see Paper I). Our optimum model spectra can be represented by a broken power law:

$$I_\nu = \begin{cases} I_{\rm H\,I}\left(\dfrac{\nu}{\nu_{\rm LL}}\right)^{-\alpha_1}; & 5 \le h\nu({\rm eV}) < 24.6, \\ I_{\rm H\,I}\left(\dfrac{\nu}{\nu_{\rm LL}}\right)^{-3}; & 24.6 \le h\nu({\rm eV}) < 54.4, \\ I_{\rm He\,II}\left(\dfrac{\nu}{\nu_{\rm He\,II}}\right)^{-\alpha_2}; & 54.4 \le h\nu({\rm eV}) < 1000, \\ I_{\rm 1keV}\left(\dfrac{\nu}{\nu_{\rm 1keV}}\right)^{-0.7}; & 1000 \le h\nu({\rm eV}) < 5000, \end{cases} \quad (1)$$

where $\nu_{\rm LL}$ and $\nu_{\rm He\,II}$ are the frequency at the H I ionization edge and He II edge, respectively; $\nu_{\rm 1keV}$ is the frequency corresponding to 1 keV. The spectral indices, α_1 and α_2, and the hydrogen Lyman limit intensity, $I_{\rm H\,I-21}$, in units of 10^{-21} erg s^{-1}cm^{-2}Hz^{-1}sr^{-1} were set as $(\alpha_1, \alpha_2, I_{\rm H\,I-21})$= (1.5, 0.26, 1.0) for the model T15Mh, (0.7, 0.26, 1.0) for the model T07Mh, and (1.5, 0.575, 0.1) for the model T15LL. All of these models have a break at the He I ionization edge (24.6 eV) in order to assure the continuity of the spectra.

We also adopted the integrated UV radiation from quasars for a comparison with our optimum models as the ionizing background radiation. Considering the intervening absorption due to H I, He I, and He II arising from the Lyman α forests and LLSs, the mean intensity I_ν of the integrated UV background at frequency $\nu_{\rm obs}$ in the rest frame of redshift $z_{\rm obs}$ was expressed as (Bechtold et al. 1987; Miralda-Escudé, Ostriker 1990, hereafter MO90; Madau 1992)

$$I_\nu(\nu_{\rm obs}, z_{\rm obs}) = \frac{c}{4\pi H_0}\int_{z_{\rm obs}}^{z_{\rm max}} \frac{(1+z_{\rm obs})^3}{(1+z)^3} \times \frac{\epsilon(\nu, z)\exp[-\tau(\nu_{\rm obs}, z_{\rm obs}, z)]}{(1+z)^2(1+2q_0 z)^{1/2}} dz, \quad (2)$$

where $\epsilon(\nu, z)$ is the proper volume emissivity in units of erg cm^{-2}s^{-1}Hz^{-1} of quasars at frequency $\nu = \nu_{\rm obs}(1+z)/(1+z_{\rm obs})$ and redshift z, and $\exp[-\tau(\nu_{\rm obs}, z_{\rm obs}, z)]$ is the mean transmission over all lines of sight to the observer at $z_{\rm obs}$. Following Madau (1992), we adopted the quasar luminosity function (LF) at $0.3 < z < 2.9$ given by Boyle (1991) and assumed that the comoving number density of quasars at $z \gtrsim 3$ is constant, and that the luminosity function at $z \simeq 2.9$ is responsible for the general properties of the quasars at $2.9 \lesssim z \lesssim 5$. We assumed the intrinsic spectrum of quasars as

$$f_\nu \propto \begin{cases} \nu^{-0.7}; & 5 \le h\nu({\rm eV}) < 10.2\ , \\ \nu^{-1.5}; & 10.2 \le h\nu({\rm eV}) < 500, \\ \nu^{-0.7}; & 500 \le h\nu({\rm eV}) < 5000\ . \end{cases} \quad (3)$$

This was based on the IUE observations reported by O'Brien et al. (1988); its power index at $\lambda < 1216$ Å is also consistent with $\alpha_{\rm ox} \simeq 1.4$, the extrapolated spectrum index from optical to X-ray bands (Zamorani et al. 1981). This is also a mimic spectrum of the "medium" quasar spectrum in Bechtold et al. (1987) and "model QS2" of MO90. Recently, Tytler et al. (1995) have used their HST images of 82 high redshift quasars, and performed Monte-Carlo simulations of the intervening absorption in order to determine the mean intrinsic spectrum of quasars in 330–1300 Å. They derived the intrinsic spectral shape as $f_\nu \propto \nu^{-1.5}$. Following Miralda-Escudé and Ostriker (1992), we took the absorption effects due to H I, He I, and He II in the Lyman α clouds and the LLSs into account. When the number of absorption lines per unit redshift per unit H I column density is expressed as $f(N_{\rm H\,I}, z)dN_{\rm H\,I}dz$, the "effective" optical depth for a photon emitted at redshift $z_{\rm em}$ and observed at redshift $z_{\rm obs}$ with frequency $\nu_{\rm obs}$ is

$$\tau(\nu_{\rm obs}, z_{\rm obs}, z_{\rm em}) = \int_{z_{\rm obs}}^{z_{\rm em}} dz \int_{N_{\rm min}}^{N_{\rm max}} dN_{\rm H\,I} f(N_{\rm H\,I}, z)[1-\exp(-\Delta)], \quad (4)$$

where $\Delta = \sum N_x \sigma_x(\nu)$ [x = H I, He I, and He II] is the optical depth of a cloud at redshift z with a neutral hydrogen column density $N_{\rm H\,I}$, and σ_x is a photoionization cross section as a function of frequency, $\nu = \nu_{\rm obs}(1+z)/(1+z_{\rm obs})$. We adopted two models for the observed distribution of Lyman α clouds and LLSs. First, $f(N_{\rm H\,I}, z)$ is the same as "model A2" from MO90,

$$f(N_{\rm H\,I}, z) = \begin{cases} 2.0\times10^7 N_{\rm H\,I}^{-1.5}(1+z)^{2.4}\ ; \\ \quad (10^{14} < N_{\rm H\,I} < 1.58\times10^{17}{\rm cm}^{-2}) \\ 2.3\times10^8 N_{\rm H\,I}^{-1.5}(1+z)^{0.5}\ ; \\ \quad (1.58\times10^{17} < N_{\rm H\,I} < 10^{22}{\rm cm}^{-2}). \end{cases} \quad (5)$$

Second, we adopted $f(N_{\rm H\,I}, z)$ based on recent observations. Bechtold (1994) derived a slower evolution law of dn/dz of the Lyman α clouds in $z_{\rm abs} \simeq$ 0–4; $dn/dz = 20.2(1+z)^{1.32\pm0.24}$ for the Lyman α lines with $W_{\rm eq} > 0.16$ Å. For the Lyman limit systems, Stengler-Larrea et al. (1995) showed a more rapid evolution in $0.32 \le z_{\rm abs} \le 4.11$; $dn/dz = 0.25(1+z)^{1.50\pm0.39}$. We calculated the coefficients in the equation of $f(N_{\rm H\,I}, z)$ following MO90. We thus set "model A3" as

$$f(N_{\rm H\,I}, z) = \begin{cases} 7.4\times10^7 N_{\rm H\,I}^{-1.5}(1+z)^{1.32}\ ; \\ \quad (10^{13} < N_{\rm H\,I} < 1.58\times10^{17}{\rm cm}^{-2}) \\ 4.97\times10^7 N_{\rm H\,I}^{-1.5}(1+z)^{1.50}\ ; \\ \quad (1.58\times10^{17} < N_{\rm H\,I} < 10^{22}{\rm cm}^{-2}). \end{cases} \quad (6)$$

We call the integrated UV background models based on two types of the modification due to the intervening absorption systems as model QA2 corresponding to model A2, and model QA3 corresponding to model A3, respectively.

We estimated the column densities of He I and He II from $N_{\rm H\,I}$ under photoionization equilibria with suitable assumptions, for simplicity. $N_{\rm He\,I}/N_{\rm H\,I}$ and $N_{\rm He\,II}/N_{\rm H\,I}$ are given by

$$\frac{N_{\rm He\,I}}{N_{\rm H\,I}} = 0.044\frac{\mathcal{I}_{\rm H\,I}}{\mathcal{I}_{\rm He\,I}}, \quad (7)$$

$$\frac{N_{\rm He\,II}}{N_{\rm H\,I}} = 1.8\frac{\mathcal{I}_{\rm H\,I}}{\mathcal{I}_{\rm He\,II}}, \quad (8)$$

where $\mathcal{I}_{\rm H\,I}$ is the frequency-averaged intensity at the H I edge, weighted by the factor $\sigma_{\rm H\,I}/\nu$; $\mathcal{I}_{\rm He\,I}$ and $\mathcal{I}_{\rm He\,II}$ are analogous quantities. Following Miralda-Escudé and Ostriker (1992), we checked the validity of these approximations. Each approximation is valid for clouds for an He I or He II optical depth on the order of unity, which mainly contributes to the corresponding absorption. The absorption by He I and He II is dominated by the clouds at different H I column densities. We could adopted these approximations to a cloud with a radius and gas density in the range of 10–100 kpc and $n_{\rm H} \lesssim 10^{-1}{\rm cm}^{-3}$. Finally, Δ in equation (4) was calculated as

$$\Delta = N_{\rm H\,I}\left[\sigma_{\rm H\,I}(\nu) + 0.044\frac{\mathcal{I}_{\rm H\,I}}{\mathcal{I}_{\rm He\,I}}\sigma_{\rm He\,I}(\nu) + 1.8\frac{\mathcal{I}_{\rm H\,I}}{\mathcal{I}_{\rm He\,II}}\sigma_{\rm He\,II}(\nu)\right]. \quad (9)$$

Our optimum spectra and spectra of the integrated UV radiations are presented in figure 1.

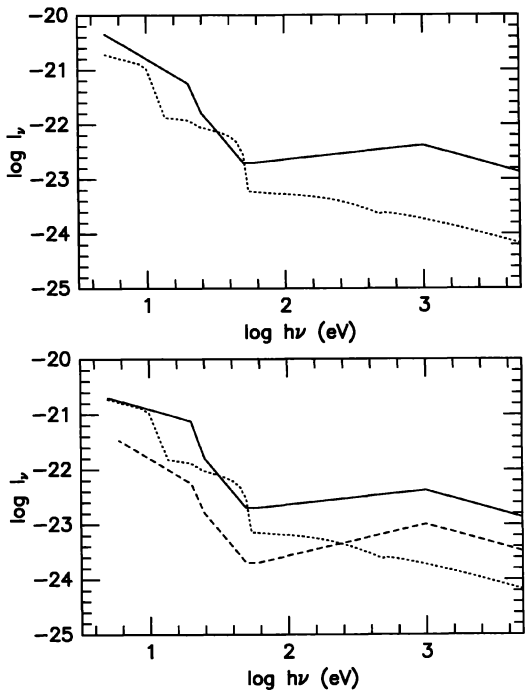

Fig. 1. Spectral shapes of the UV background models. In the upper panel, the optimum model spectrum T15Mh (solid line) and the integrated model spectrum QA2 (dotted line) are presented. In the lower panel, the model spectra T07Mh (solid line) and T15Ll (dashed line), and the integrated model spectrum QA3 (dotted line) are presented.

2.2. *Gaseous Clouds at High Redshifts*

We assume that the Lyman α forest arises in gas clouds of subgalactic mass scale confined by the gravity of dark-matter halos. Instead of solving the dynamics of such clouds, we refer to the results studied by Ikeuchi et al. (1989) and Murakami and Ikeuchi (1993) on the basis of the 'minihalo model'. For simplicity, an absorber is assumed to have te following gas-density distribution:

$$n_{\rm H}(r) = \begin{cases} n_0 & ; 0 \le r \le r_0, \\ n_0 (r/r_0)^{-2} & ; r_0 \le r \le R, \\ 0 & ; r > R. \end{cases} \quad (10)$$

Here, $r_0 \simeq 1.6$ kpc and R, the radius of a model cloud, is fixed at $R = 100$ kpc, independent of its mass. The radius of the gaseous cloud in the gravitational equilibrium has such a weak dependence on its mass, $R \propto M^x$ with $x \sim 0.125$ (Ikeuchi et al. 1989), that we can safely neglect this dependence.

The total gas mass is expressed as $M/M_\odot = 8.3 \times 10^{10} (n_0/1\ {\rm cm}^{-3})$ and the total hydrogen column density along the line of sight penetrating the center of the model cloud is $N_{\rm H} = 2.0 \times 10^{22} (n_0/1\ {\rm cm}^{-3})\ {\rm cm}^{-2}$. We consider absorbers with gas masses in the range of $M/M_\odot = 10^8$–10^{10}, and assume that the cloud mass function can be represented by the following power-law form:

$$\frac{dn_{\rm c}}{dM} \propto \left(\frac{M}{M_*}\right)^{-\delta} d\left(\frac{M}{M_*}\right); \delta = 1.5, 2.0, 2.5, 3.0. \quad (11)$$

Here, M_* is assumed to be $10^{10} M_\odot$. Note that the results do not change crucially when the range of the gas masses is adopted as $M/M_\odot = 10^8$–10^{11}.

The abundance of all elements heavier than helium is assumed to be 1×10^{-2} of the solar value (Allen 1973), which is consistent with the observations (Cowie et al. 1995). The helium abundance is set to one ninth of the hydrogen atom in number. We solved the equations of the ionization equilibria and the thermal equilibrium self-consistently, and then obtained the ionization states of the absorbers (for details, see Denda, Ikeuchi 1993 and references therein).

We calculated the column density of each ion X_i (= H I, He I, and He II), $N(X_i)$, along the line of sight at an impact parameter p as

$$N(X_i) = 2 \int_p^R \frac{n_{X_i}(r) r}{\sqrt{r^2 - p^2}} dr, \quad (12)$$

where $n_{X_i}(r)$ is the spatial number density of X_i. The number of absorbers observed in both $(z, z + dz)$ and $(N_{X_i},\ N_{X_i} + dN_{X_i})$ is written as (e.g., Rees 1988)

$$\frac{d^2 n}{dN_{X_i} dz} dN_{X_i} dz = n_{\rm g}(z, M) \pi \left|\frac{pdp}{dN_{X_i}}\right| \left|\frac{dl}{dz}\right| dN_{X_i} dz, \quad (13)$$

where $n_{\rm g}(z, M)$ represents the spatial density of the gas clouds as a function of the mass M and redshift z. We assumed that the comoving number density of the absorbers is constant, and that their mass function can be represented by a power-law form, as in equation (11), and then integrated with mass,

$$\frac{d^2 \mathcal{N}}{dN_{X_i} dz} = \frac{c \pi n_{\rm g}(M_*)}{H_0} \int \left|\frac{pdp}{dN_{X_i}}\right| \left(\frac{M}{M_*}\right)^{-\delta} \times d\left(\frac{M}{M_*}\right) (1+z)^{1-q_0}. \quad (14)$$

This equation is valid only for $q_0 = 0$ or 0.5. We set $q_0 = 0.5$ throughout this paper. To make a comparison with observations, we calculated the z-integrated ion column-density distribution that is integrated over observed redshift range, and then averaged by the "absorption distance" defined by Tytler (1987) and Sargent et al. (1989),

$$\frac{d\mathcal{N}}{dN_{X_i}} = \int_0^{z_{\rm max}} \frac{d^2 \mathcal{N}}{dN_{X_i} dz} dz \Big/ \left\{\frac{(1+z_{\rm max})^{2-q_0} - 1}{2 - q_0}\right\}. \quad (15)$$

In this study, the value of $n_g(M_*)$ was assumed to be a free parameter in order that the calculated $d\mathcal{N}/dN_{\rm H\,I}$ would fit the observed value (Hu et al. 1995) around $\log N_{\rm H\,I} = 14$.

3. Ionization States of the Lyman α Clouds

3.1. *Column-Density Distribution of H I, He I, and He II*

The observed column-density distribution is usually presented as a power law form,

$$\frac{dn}{dN_{X_i}} \propto N_{X_i}^{-\beta_{X_i}}. \tag{16}$$

Using a low-resolution sample, Tytler (1987) found that in the range of $10^{13} < N_{\rm H\,I} < 10^{22}{\rm cm}^{-2}$ the observed numbers per unit H I column density are reasonably well represented by a single power law, $dn/dN_{\rm H\,I} \propto N_{\rm H\,I}^{-\beta_{\rm H\,I}}$ with $\beta_{\rm H\,I} = 1.51 \pm 0.02$. Sargent et al. (1989) also found a similar power-law fitting with $\beta_{\rm H\,I} = 1.51 \pm 0.02$ for $13.25 \leq \log N_{\rm H\,I} \leq 22.0$ at $\langle z_{\rm abs}\rangle = 1.957$. On the other hand, Bechtold (1988) found that a single power law gives a poor fit to the data. She found very different indices for $N_{\rm H\,I} < 10^{16}{\rm cm}^{-2}$ and $N_{\rm H\,I} > 10^{16}{\rm cm}^{-2}$, $\beta_{\rm H\,I} = 1.6 \pm 0.1$ and 0.8 ± 0.1, respectively. At the high column-density edge, $10^{17.2} < N_{\rm H\,I} < 10^{21.8}{\rm cm}^{-2}$, Lanzetta (1991) found $\beta_{\rm H\,I} = 1.25 \pm 0.03$. Recently, Petitjean et al. (1993) has shown that $dn/dN_{\rm H\,I}$ cannot be fit either by a single or a double power law, using a high resolution sample, and that there is a flattening at $N_{\rm H\,I} \simeq 10^{16}{\rm cm}^{-2}$, which can be explained in terms of a transition between the Lyman α clouds and the metallic absorption system. Hu et al. (1995) revealed that the observed column-density distribution can be expressed as a single power-law form with $dn/dN_{\rm H\,I} \propto N_{\rm H\,I}^{-1.46}$; the power-law index, $\beta_{\rm H\,I} = 1.37$–1.51, with a 95% confidence level in the column-density range of $2 \times 10^{12} \leq N_{\rm H\,I}({\rm cm}^{-2}) \leq 3 \times 10^{14}$. They also reported that there is indeed a significant steepening in the slope of $dn/dN_{\rm H\,I}$ above $N_{\rm H\,I} = 3 \times 10^{14}{\rm cm}^{-2}$. It has been gradually revealed that there are some structures in the H I column-density distribution of the quasar absorption systems.

The numerical results are shown in figure 2. We omit a discussion about the results obtained by model T07Mh in this subsection, because models T15Mh and T07Mh predict almost the same $dn/dN_{\rm H\,I}$. It is clearly shown in figure 2 that all of the resultant $dn/dN_{\rm H\,I}$ have a similar distribution, independent of the shape of the ionizing spectrum. More precisely, model T15Mh predicts a slightly steeper slope of the H I column-density distribution than do the other spectra. Because model T15Mh has a larger hydrogen Lyman-limit intensity by a factor of 10 than the other models, it predicts a higher ionization state. The absorbing clouds in a high ionization level have a small minimum $N_{\rm H\,I}$ along the line of sight at the largest impact parameter. The probability of incidence therefore increases at the lower $N_{\rm H\,I}$ end, but decreases at the higher $N_{\rm H\,I}$ end. The higher ionization level of the absorbing clouds thus shows the steeper slope of $dn/dN_{\rm H\,I}$. On the other hand, model T15Ll, which predicts the lowest ionization state among our photoionization models, obtains a somewhat flatter slope of $dn/dN_{\rm H\,I}$ (see figure 3).

Our photoionization models can probably explain the observed $dn/dN_{\rm H\,I}$ in the range of $N_{\rm H\,I} \simeq 2 \times 10^{12}$–$10^{15}{\rm cm}^{-2}$ with the index of the mass function being $\delta = 1.5$–2 (see figures 2 and 3).

The resultant slopes of the H I column-density distribution with the index of the mass function, $\delta = 1.5$, are $\beta_{\rm H\,I} = 1.55 \pm 0.01$ for model T15Mh, $\beta_{\rm H\,I} = 1.41 \pm 0.02$ for model T15Ll, $\beta_{\rm H\,I} = 1.45 \pm 0.02$ for model QA2, and $\beta_{\rm H\,I} = 1.46 \pm 0.02$ for model QA3, respectively. However, a mass function of the Lyman α clouds with a steeper slope cannot be ruled out here. If the observed slope is steeper than that obtained by Hu et al. (1995), as reported by Bechtold (1988), the allowed range of the index of the cloud mass function would become wider toward larger δ. Such a situation is possible, because many populations of weak Lyman α clouds may be undetected, even with HIRES. On the other hand, our photoionization models can reproduce neither the significant steepening of the slope of the $dn/dN_{\rm H\,I}$ above $N_{\rm H\,I} = 3 \times 10^{14}{\rm cm}^{-2}$ reported by Hu et al. (1995), nor the flattening at $N_{\rm H\,I} \simeq 10^{16}{\rm cm}^{-2}$ pointed out by Petitjean et al. (1993). The absorbers modeled here have an identical gas-density distribution, and are in almost homogeneous and high-ionization level. Such clouds thus do not show any variation in the slope of the $dn/dN_{\rm H\,I}$ due to the inhomogeneity of the ionization state dependent on the distance from the center of the gaseous clouds.

We present the resultant column-density distribution of He I and He II in figure 4. Because all of the photoionization models predict similar column-density distributions of He I and He II, the results obtained by model QA3 are presented as an example. Both column-density distributions can be fit by a power-law distribution as well as $dn/dN_{\rm H\,I}$, while their power-law indices are generally smaller than that of $dn/dN_{\rm H\,I}$: $\beta_{\rm He\,I} \sim \beta_{\rm H\,I} - 0.12$, $\beta_{\rm He\,II} \sim \beta_{\rm H\,I} - 0.25$ for all models. These feature will be confirmed in future observations. Figure 3 shows the calculated slopes, β_{X_i} (X_i = H I, He I, and He II), as a function of the index of the cloud mass function δ.

3.2. *C IV/H I Ratio*

The traditional view of the Lyman α forest is intergalactic clouds of primordial composition (Sargent et al. 1980). If the Lyman α clouds consist of primordial gas, their formation and evolution were probably different from those of galaxies. It is thus crucial to search for metal absorption lines associated with the Lyman α

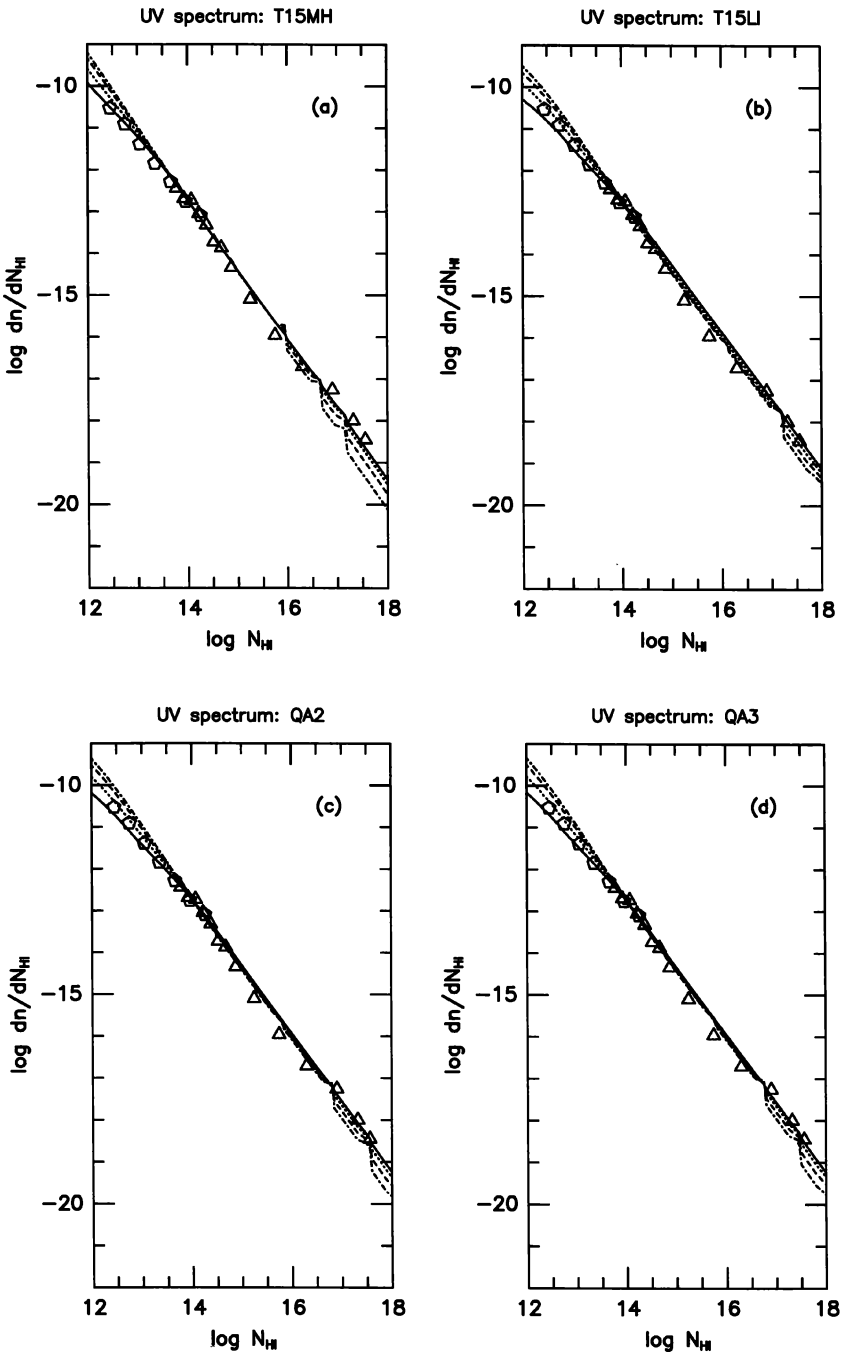

Fig. 2. Resultant H I column-density distribution. The mass function of the Lyman α clouds is assumed to be $dn/dM_c \propto M_c^{-\delta}$; $\delta = 1.5$ (solid line), $\delta = 2.0$ (dotted line), $\delta = 2.5$ (dashed line), and $\delta = 3.0$ (dot-dash line). The UV spectra are (a) model T15Mh, (b) model T15Ll, (c) model QA2, and (d) model QA3. The resultant slopes of the H I column-density distribution with the index of the mass function $\delta = 1.5$ are $\beta_{\rm H\,I} = 1.55 \pm 0.01$ for model T15Mh, $\beta_{\rm H\,I} = 1.41 \pm 0.02$ for model T15Ll, $\beta_{\rm H\,I} = 1.45 \pm 0.02$ for model QA2, and $\beta_{\rm H\,I} = 1.46 \pm 0.02$ for model QA3, respectively. Note that normalization is performed at $N_{\rm H\,I} = 10^{14}{\rm cm}^{-2}$ in order that the calculated $dn/dN_{\rm H\,I}$ can fit the observed one by Hu et al. (1995). The observed data are adopted from Petitjean et al. (1993; open triangle) and Hu et al. (1995; open pentagon).

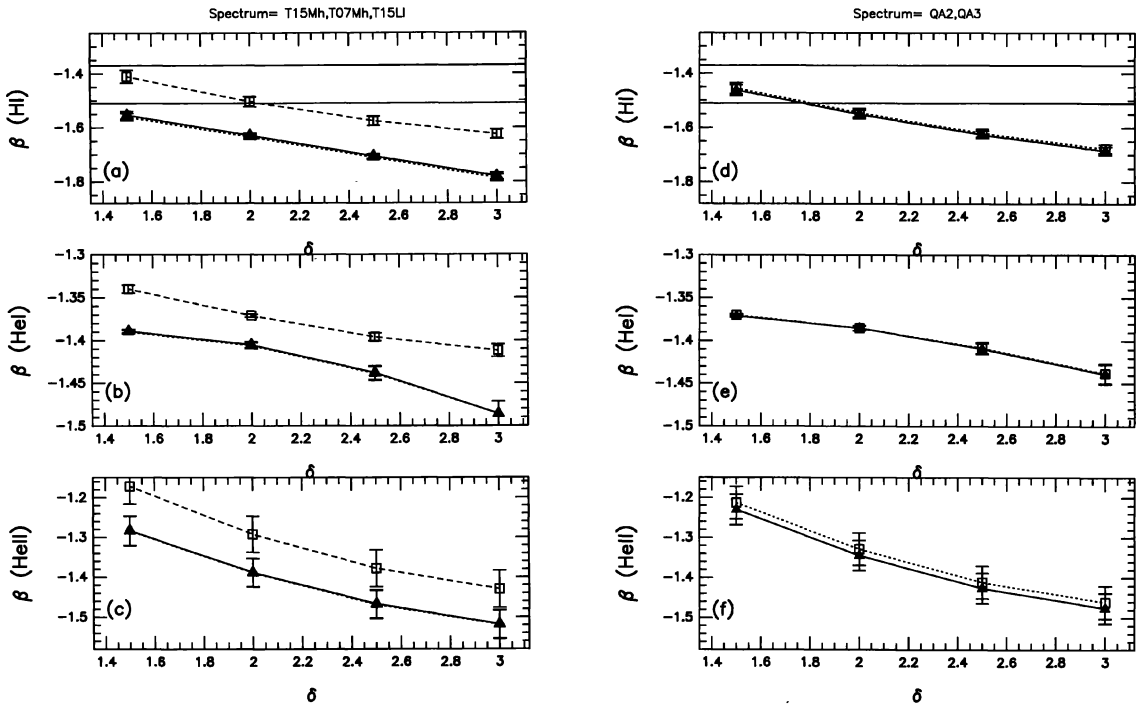

Fig. 3. Resultant slopes of the column-density distributions. In (a), (b), and (c), the solid line with filled triangles indicates the result obtained by model T15Mh, the dashed line with open squares model T15Ll, respectively. The results predicted by model T15Mh are the same as those obtained by model T07Mh. In (d), (e), and (f), the solid line with filled triangles indicates the results obtained by model QA3, and the dotted line with open squares model QA2. These results indicate that the spectrum with a stronger hydrogen Lyman-limit intensity predicts a steeper column-density distribution of each ion. The allowed range obtained by Hu et al. (1995) of β (H I) is between the two horizontal lines shown in (a) and (d).

forest in order to study the origin of those absorbers. Composite spectrum methods (Norris et al. 1983) have been used to obtain the mean equivalent width of the metal absorption lines corresponding to the Lyman α forest in order to derive the mean metallicity of such absorption systems. Lu (1991) reported a significant detection of the column-density ratio, $\langle \mathrm{C\,IV/H\,I} \rangle = 7 \times 10^{-4}$, for cloud populations with $N_{\mathrm{H\,I}} \geq 2.45 \times 10^{15} \mathrm{cm}^{-2}$, and obtained [C/H] ~ -3.1 at $\langle z \rangle \simeq 2.6$. With a much higher S/N, the higher-resolution spectra obtained by the HIRES on the Keck telescope have revealed that roughly half of a population of the Lyman α clouds with $N_{\mathrm{H\,I}} \geq 3 \times 10^{14} \mathrm{cm}^{-2}$ can be associated with the metal absorption lines of $N_{\mathrm{C\,IV}} \geq 10^{12} \mathrm{cm}^{-2}$ (Cowie et al. 1995). They found $\langle \mathrm{C\,IV/H\,I} \rangle = 3 \times 10^{-3}$ in the range of $10^{14} \leq N_{\mathrm{H\,I}} \leq 5 \times 10^{15} \mathrm{cm}^{-2}$, roughly corresponding to a metallicity of 10^{-2} solar abundance at $\langle z \rangle = 2.6$. Moreover, Tytler et al. (1995) found that all of the Lyman α absorption systems with $N_{\mathrm{H\,I}} > 10^{15} \mathrm{cm}^{-2}$ and 60% of those systems with $N_{\mathrm{H\,I}} > 10^{14.5} \mathrm{cm}^{-2}$ have shown corresponding C IV absorption lines at $\langle z \rangle \simeq 2.8$.

The ratio of C IV/H I depends on both the metallicity and the shape of the ionizing spectrum, when the absorbing gas is photoionized. We then examined whether or not our photoionization models reproduce the observed C IV/H I ratio, and present the results in figure 5. The observed data are referred from Cowie et al. (1995) and references therein. Clearly, figure 5 shows that the integrated UV background models (models QA2 and QA3) explain the observations well. When a total gas mass of $M \simeq 6 \times 10^{8}$–$10^{10} M_{\odot}$ is irradiated by model spectra QA2 or QA3, such an absorber can explain the C IV/H I ratio of both the Lyman α forest and LLSs, simultaneously. On the other hand, the broken power-law models (models T15Mh, T07Mh, and T15Ll) predict lower C IV/H I ratios than those observed; for model T15Mh, $[\mathrm{C\,IV/H\,I}]_{\mathrm{cal}} = 0.5\ [\mathrm{C\,IV/H\,I}]_{\mathrm{obs}}$ in the range of $10^{14} \leq N_{\mathrm{H\,I}} \leq 5 \times 10^{15} \mathrm{cm}^{-2}$. Especially, model T15Ll predicts the lowest C IV/H I ratio at the peak value among these broken power-law models, because of the weakest intensity of the ionizing radiation. It is possible to modify the results to fit the observed data with larger metallicity,

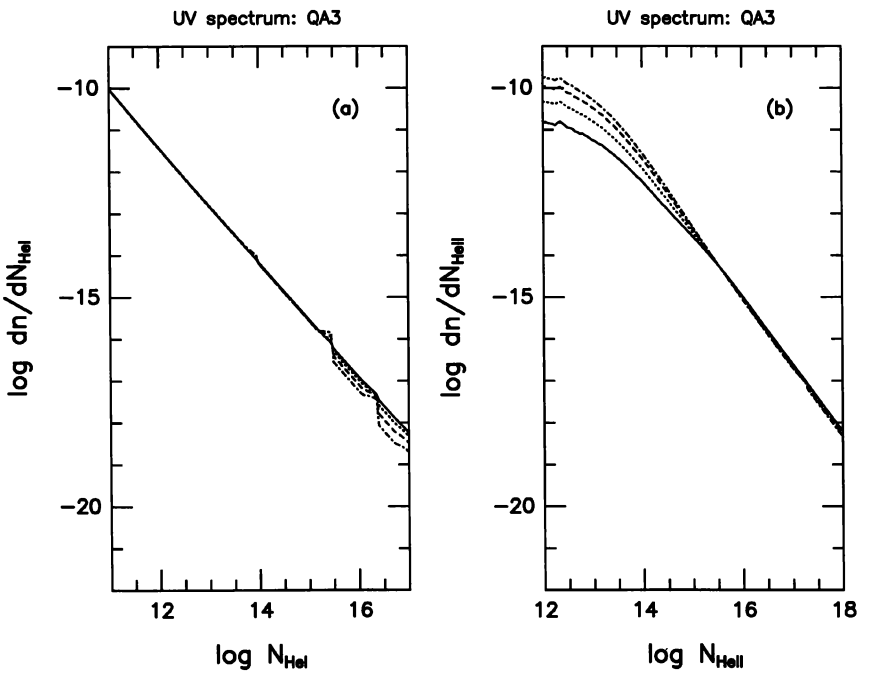

Fig. 4. Resultant helium column-density distribution predicted by model QA3. Each panel shows (a) for the He I column-density distribution, and (b) for the He II distribution. The mass function of the Lyman α clouds is assumed to be $dn/dM_c \propto M_c^{-\delta}$; $\delta = 1.5$ (solid line), $\delta = 2.0$ (dotted line), $\delta = 2.5$ (dashed line), and $\delta = 3.0$ (dot-dash line).

e.g., 3×10^{-2} solar abundance. However, model T15Ll has almost the same hydrogen Lyman-limit intensity $I_{\nu_{LL}}$ as those of models QA2 and QA3, although the spectral shape is different. Models QA2 and QA3 have an excess in the energy band between the H I edge and the He II edge compared with the broken power-law models. We therefore infer that the shape of the ionizing radiation is more important than the metallicity to explain the observed C IV/H I ratio of the Lyman α clouds. The suitable UV radiation should have a flat spectrum in the energy-band range of 13.6–54.4 eV and a break at the He II edge rather than a steep spectrum in the relevant energy range.

4. Optical Depth of the Universe

4.1. Line-Blanketing Effect

As for the H I optical depth due to the Lyman α clouds, Songaila et al. (1995) reported that in their spectrum of quasar Q0302−003 the mean optical depth is $\langle \tau^c_{H\,I} \rangle = 0.31$ between 4500 and 5000 Å, in which wavelengths of the redshifted Lyman α lines correspond to the redshift range of $z \simeq 2.7$–3.1. Davidsen et al. (1996) measured the H I absorption in the low-resolution spectrum of HS 1700+6416, and obtained $\tau^c_{H\,I} = 0.22$ at $\langle z \rangle = 2.4$. The other observations of the intergalactic H I absorption at $z \sim 2.6$–4 have inferred $\tau_{H\,I} = 0.35 \pm 0.1$ (Steidel, Sargent 1987; Schneider et al. 1991; Webb et al. 1992). We adopted $\tau^c_{H\,I} \simeq 0.22$ at $z = 2.2$–2.6 and $\tau^c_{H\,I} \simeq 0.3$ at $z = 2.6$–3.0 as the observational limits.

As for the He II optical depth, Jakobsen et al. (1994) reported a tentative detection of the He II Gunn-Peterson optical depth at $z \sim 3$ with the FOC/HST. The 90% confidence bound on the He II optical depth gives the lower limit as $\tau^c_{He\,II} > 1.7$ at $z \simeq 3.2$ on the line of sight to quasar Q0302−003. Tytler et al. (1995) detected the He II optical depth, $\tau_{He\,II} = 1.0 \pm 0.2$, at $z \simeq 3.1$ in the spectrum of the quasar Q1935−69 with the FOS/HST. They pointed out that the spectrum of Jakobsen et al. (1994) is doubtful because it shows a strong emission line just redward of redshifted 304 Å, at which no emission lines appear in the spectra of Tytler et al. (1995), and no emission lines are expected from the standard photoionization models. Although these detections may conflict with each other, there is a possibility that both results are correct. The IGM probably shows inhomogeneous ionization state, because the epoch of ionization of He II may be later than that of H I (Miralda-Escudé, Rees 1994). Otherwise, quasar Q1935−69, itself, possibly radiates many He II ionizing photons, enhancing its He II

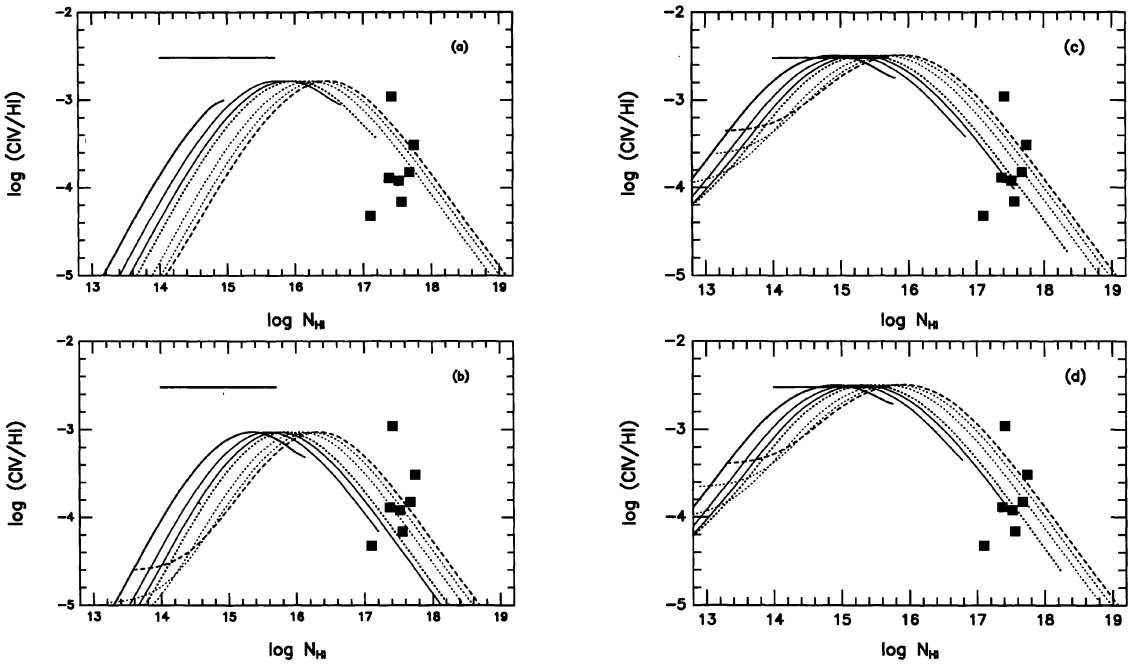

Fig. 5. Column-density ratio of C IV/H I vs. H I column density. Each panel shows (a) for model T15Mh, (b) for model T15Ll, (c) for model QA2, and (d) for model QA3. The horizontal line and filled squares in each figure show the observed values for the Lyman α forest and the LLSs given by Cowie et al. (1995) and reference therein. Each curve indicates the result obtained by an absorber with a gas mass of 10^8, 3×10^8, 6×10^8, 10^9, 3×10^9, 6×10^9, and $10^{10}M_\odot$ from left to right.

proximity effect up to the extent that the He II optical depth decreases (Giroux et al. 1995). However, the spectrum taken by Tytler et al. (1995) may be affected by scattered light in the spectrograph at the relevant wavelengths. More recently, Davidsen et al. (1996) observed quasar HS 1700+6416 with the Hopkins Ultraviolet Telescope (HUT) on board the Space Shuttle, and found the effective He II optical depth, $\tau_{\rm He\,II}=1.00\pm0.07$, at the mean absorption redshift of $z=2.4$. It may be a more certain measurement of the He II optical depth than the other two detections, even though the relevant redshifts are slightly different. We adopted $\tau^{\rm c}_{\rm He\,II}\geq1.0$ at $z\sim3$ as a lower limit to the He II optical depth due to the line blanketing of the Lyman α clouds, and $\tau^{\rm c}_{\rm He\,II}=1.00\pm0.07$ in the redshift range $2.2<z<2.6$.

In the spectral region shortward of the quasar's Lyman α emission line of H I, He I, or He II, the continuum radiation is attenuated by the blanketing effect of many absorption lines arising in the intervening absorption systems. The average transmission over all lines of sights may be expressed as $\langle e^{-\tau}\rangle\equiv e^{-\tau_{\rm eff}}$ with the effective optical depth $\tau_{\rm eff}$ given by

$$\tau_{\rm eff}(z)=\frac{1+z}{\lambda_\alpha}\int_{W_{\rm min}}^{W_{\rm max}}\frac{d^2\mathcal{N}}{dWdz}WdW, \tag{17}$$

where λ_α is the vacuum wavelength of the Lyman α line of H I, He I, or He II and $d^2\mathcal{N}/dWdz$ is the rest equivalent-width distribution of each ion (Paresce et al. 1980; Madau, Meiksin 1994). The absorption systems are assumed to follow a Poissonian spatial distribution. Using the relation between the equivalent width distribution and the column density distribution,

$$\frac{d^2\mathcal{N}}{dWdz}dW=\frac{d^2\mathcal{N}}{dNdz}dN, \tag{18}$$

we can rewrite equation (17) as

$$\tau_{\rm eff}(z)=\frac{1+z}{\lambda_\alpha}\int_{N_{\rm min}}^{N_{\rm max}}\frac{d^2\mathcal{N}}{dNdz}W(N,b)dN. \tag{19}$$

The equivalent width W is a function of both the column density N and the Doppler parameter b through a curve of growth. When we calculated the rest equivalent width W, which corresponds to the column density N, through the curve of growth, we set the Doppler parameter of hydrogen Lyman α line as $b_{\rm H\,I}=34\,{\rm km\ s^{-1}}$, which was averaged in the Lyman α forest (Carswell et al. 1991). Moreover, we used the ratio of the Doppler parameter of the helium line to that of hydrogen, $\zeta=b_{\rm He\,II}/b_{\rm H\,I}$, to evaluate the line width of He II ($\zeta=0.5$ is for pure thermal broadening, and $\zeta=1$ is for turbulent broadening).

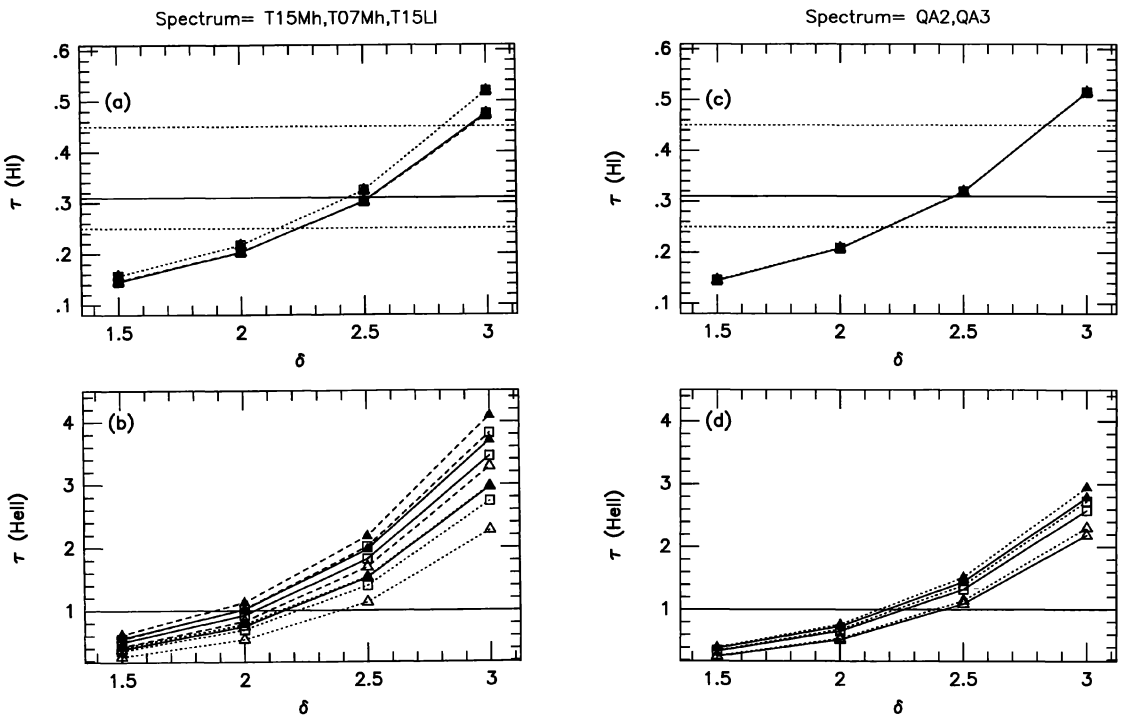

Fig. 6. Line-blanketing optical depths as a function of the power-law index of the mass function of the Lyman α clouds. (a) and (c) show the H I optical depth. The horizontal solid line corresponds to the mean H I optical depth due to the Lyman α clouds obtained by Songaila et al. (1995), and the region between the horizontal dotted lines indicates the observed range (Steidel, Sargent 1987; Schneider et al. 1991; Webb et al. 1992). Solid lines in (a) and (b) show model T15Mh, dotted lines for model T15Ll, and dashed lines for model T07Mh. In (b) and (d), the He II optical depth is shown. The horizontal line shows the lower limit. The Doppler parameter ratio, $\zeta = b_{\rm He\,II}/b_{\rm H\,I}$, is assumed to be $\zeta = 0.5$ (pure thermal broadening; open triangle), $\zeta = 0.8$ estimated by Cowie et al. (1995; open square), and $\zeta = 1.0$ (turbulent broadening; filled square). In (c) and (d), the solid line concerns model QA3, and the dotted line model QA2.

Cowie et al. (1995) analyzed the velocity structures of the C IV lines corresponding to the Lyman α lines, and found that the turbulent broadening and the thermal broadening are nearly equal in the Lyman α clouds, indicating $\zeta \simeq 0.8$. Therefore, $\zeta = 0.5$, 0.8, and 1.0 were considered in our calculation. The Doppler parameter of He I Lyman α line was assumed to be equal to that of He II line. Note that the Doppler parameter of each ion was assumed to be identical for all clouds.

We calculated the column density distribution of each ion by equation (14) as described in section 3. In order to calculate the effective optical depths of H I, He I, and He II due to the Lyman α clouds, we set $N_{\rm max}$ of each ion as the column density corresponding to the maximum neutral hydrogen column density of the Lyman α clouds, at which the absorbing clouds begin to be optically thick at the hydrogen Lyman limit to the ionizing radiation, i.e., $N_{\rm H\,I,max} = 10^{17}{\rm cm}^{-2}$, and $N_{\rm min}$ of each ion corresponding to the minimum observable neutral hydrogen density, i.e., $N_{\rm H\,I,min} = 2 \times 10^{12}{\rm cm}^{-2}$ (Hu et al. 1995). However, even if the contribution from LLSs was taken into account, i.e., $N_{\rm H\,I,max} = 3 \times 10^{19}{\rm cm}^{-2}$ was adopted, the resultant optical depths were within several percentages difference from those caused only by the Lyman α clouds. We therefore restrict our discussion about the results when $N_{\rm H\,I,max} = 10^{17}{\rm cm}^{-2}$ is adopted. We do not discuss the He I blanketing effect, because all of the resultant $\tau_{\rm He\,I}$ are negligible.

The numerical results are presented in figures 6a–d, which show that the resultant optical depths are increasing functions of the power index of the mass function of the absorbing clouds δ. When the steeper mass function is adopted, the population with a lower mass dominates. Such a population with a lower mass is mainly observed in a lower $N_{\rm H\,I}$ range, which is the main contributor to the optical depth. Since the larger δ is adopted, the larger optical depth is obtained. As shown in figures 6a and 6c, the resultant $\tau^{\rm c}_{\rm H\,I}$ scarcely depends on the shape of the UV background model, but slightly depends on the hydrogen Lyman-limit intensity. In order to explain the

observational constraint on $\tau^{c}_{\rm H\,I}$, the Lyman α clouds are required to follow a somewhat steep mass function with a power-law index of $\delta \simeq 2.0 - 2.8$; $\delta = 2.5$ is the best case at $z \sim 3$, but $\delta = 2.0$ at $z \sim 2.4$. The Lyman α clouds with a mass function of $\delta = 2.5$ can satisfy the condition $\tau^{c}_{\rm He\,II} \geq 1$ at $z \simeq 3$, even when He II lines are assumed to be broadened by purely thermal motion, i.e., $\zeta = 0.5$ (open triangle in figures 6b and 6d). However, the Lyman α clouds with $\delta = 2.0$ cannot reproduce the observed He II opacity at $z \simeq 2.4$. For example, we quote the results predicted by model QA2. In the redshift range $2.2 \leq z \leq 2.6$, the mass function with $\delta = 2.0$ satisfies $\tau^{c}_{\rm H\,I}(= 0.21)$, but $\tau^{c}_{\rm He\,II} < 1$ even if the turbulent broadening is assumed ($\zeta = 1$). If $\delta = 2.5$ is adopted, the resultant $\tau^{c}_{\rm H\,II}(= 0.32)$ is somewhat larger than the observation, but $\tau^{c}_{\rm He\,I} \simeq 1$ even if the pure thermal broadening is assumed ($\zeta = 0.5$). On the other hand, the mass function with $\delta = 2.5$ reproduces $\tau^{c}_{\rm H\,I}(= 0.32)$ and predicts $1 < \tau^{c}_{\rm He\,II} \lesssim 1.5$ in the redshift range $2.6 \leq z \leq 3.0$.

When a contribution of weaker Lyman α lines to the line blanketing is included (i.e., $N_{\rm H\,I,min} = 10^{11}{\rm cm}^{-2}$), a mass function with a somewhat smaller power-law index ($\delta \gtrsim 2$) can explain the observed line-blanketing opacities of H I and He II. However, the resultant $\tau^{c}_{\rm He\,II}$ does not increase significantly, even if the weaker Lyman α lines are included. This suggests that numerous weaker Lyman α clouds are required in order that the line-blanketing effect fulfills the observed He II optical depth at $z \sim 2$–3. If the real He II optical depth at $z \sim 3$ is higher than those adopted here, the required power-law index δ becomes larger. When the lower limit of the He II optical depth is 3, the index $\delta > 2.8$ is needed in order that models T15Mh and T07Mh can explain such a large $\tau_{\rm He\,II}$. Model T15Ll and the integrated UV background models (QA2 and QA3) cannot explain such a large $\tau_{\rm He\,II}$, even if a steep mass function with $\delta = 3$ is adopted. Any other source of opacity, a substantial diffuse IGM, very weak Lyman α clouds with $N_{\rm H\,I} < 10^{12}{\rm cm}^{-2}$, or both are then necessary.

As another possibility, the UV background radiation may have a softer shape and fewer He II ionizing photons. In order that the line-blanketing effect can account for the majority of the intervening absorption, Madau and Meiksin (1994) as well as Giroux et al. (1995) showed that $\eta = N_{\rm He\,II}/N_{\rm H\,I} \sim 100$ is needed, even if the clouds are velocity broadened, and even if clouds down to $N_{\rm H\,I} = 10^{12}{\rm cm}^{-2}$ are included. On the other hand, our spectral models show a somewhat small η: $\eta \simeq 38$ (model QA2), 36 (model QA3), 52 (model T15Mh), 60 (model T07Mh), and 44 (model T15Ll), respectively.

4.2. Optical Depth Due to the IGM

For a comparison with the optical depths due to the line-blanketing effect, we also calculated the optical depths due to the IGM, i.e., the Gunn-Peterson optical depths of H I, He I, and He II. First, we briefly describe the observational limits on the Gunn-Peterson trough, and then summarize our results.

Several groups have attempted to obtain $\tau^{\rm GP}_{\rm H\,I}$ at a high redshift using the continuum depression $D_{\rm A}$, which is defined as the fractional decrement between the Lyman α and Lyman β emission lines of quasars (Oke, Korycansky 1982),

$$D_{\rm A} = \left\langle 1 - \frac{f_\nu({\rm obs})}{f_\nu({\rm cont})} \right\rangle, \tag{20}$$

where f_ν(obs) is the observed flux and f_ν(cont) is a continuum level extrapolated from redward of the Lyman α emission (Steidel, Sargent 1987; Jenkins, Ostriker 1991; Schneider et al. 1991). They then calculated the expected contribution $D_{\rm L}$ of the discrete absorption systems to $D_{\rm A}$ (Paresce et al. 1980; Meiksin, Madau 1993),

$$D_{\rm L} = 1 - \frac{1}{\Delta z}\int_{z_{\rm min}}^{z_{\rm max}} \exp[-\tau^{c}_{\rm H\,I}(z)]dz, \tag{21}$$

where $\Delta z = z_{\rm max} - z_{\rm min}$, $1 + z_{\rm max} = 0.9624\,(1 + z_{\rm em})$, $1 + z_{\rm min} = (27/32)(1 + z_{\rm em})$, and $z_{\rm em}$ is the quasar redshift. The effective optical depth $\tau^{c}_{\rm H\,I}(z)$ due to the absorption systems is given by equation (17). Clearly, the resultant $\tau^{\rm GP}_{\rm H\,I}$ depends on both the spatial and column-density distribution of the Lyman α clouds through the estimate of $D_{\rm L}$. Because $D_{\rm A}$ is given by

$$D_{\rm A} = 1 - \frac{1}{\Delta z}\int_{z_{\rm min}}^{z_{\rm max}} \exp\left[-\tau^{\rm GP}_{\rm H\,I}(z) - \tau^{c}_{\rm H\,I}(z)\right] dz, \tag{22}$$

the Gunn-Peterson optical depth in the limit $\tau^{\rm GP}_{\rm H\,I} \ll 1$ can be expressed as

$$\langle \tau^{\rm GP}_{\rm H\,I}(z) \rangle \simeq \frac{D_{\rm A} - D_{\rm L}}{1 - D_{\rm L}}. \tag{23}$$

Steidel and Sargent (1987) found a 1σ upper limit of $\tau^{\rm GP}_{\rm H\,I} < 0.05$ at $\langle z_{\rm abs} \rangle = 2.64$ using $\langle \tau^{\rm GP}_{\rm H\,I} \rangle = D_{\rm A} - D_{\rm L}$, instead of equation (23). For a larger sample of quasars, Jenkins and Ostriker (1991) have placed the 1σ limits on $\tau^{\rm GP}_{\rm H\,I} < 0.11$ at $\langle z_{\rm abs} \rangle = 2.7$ and $\tau^{\rm GP}_{\rm H\,I} < 0.31$ at $\langle z_{\rm abs} \rangle = 3.8$. On the other hand, Giallongo, Cristiani, and Trevese (1992) presented a direct measurement of the Gunn-Peterson optical depth in the spectrum of the quasar Q2126−158 ($z_{\rm em} = 3.27$). They analyzed the spectral regions in the Lyman α forest of the quasar, where strong absorption lines were absent, and then obtained the average Gunn-Peterson optical depth as simply $\tau^{\rm GP}_{\rm H\,I} = -\ln\langle f_\nu({\rm obs})/f_\nu({\rm cont})\rangle$. Their best estimate is $\tau^{\rm GP}_{\rm H\,I} = 0.013 \pm 0.026$ at $\langle z_{\rm abs} \rangle = 3$. Considering the uncertainties in the estimation of $D_{\rm L}$, we adopted the 1σ upper limit of $\tau^{\rm GP}_{\rm H\,I} < 0.05$ at $z \simeq 2.6$ and $\tau^{\rm GP}_{\rm H\,I} < 0.04$ at $z \simeq 3$ as the observational limit of the H I Gunn-Peterson optical depth. As for the He I Gunn-Peterson optical

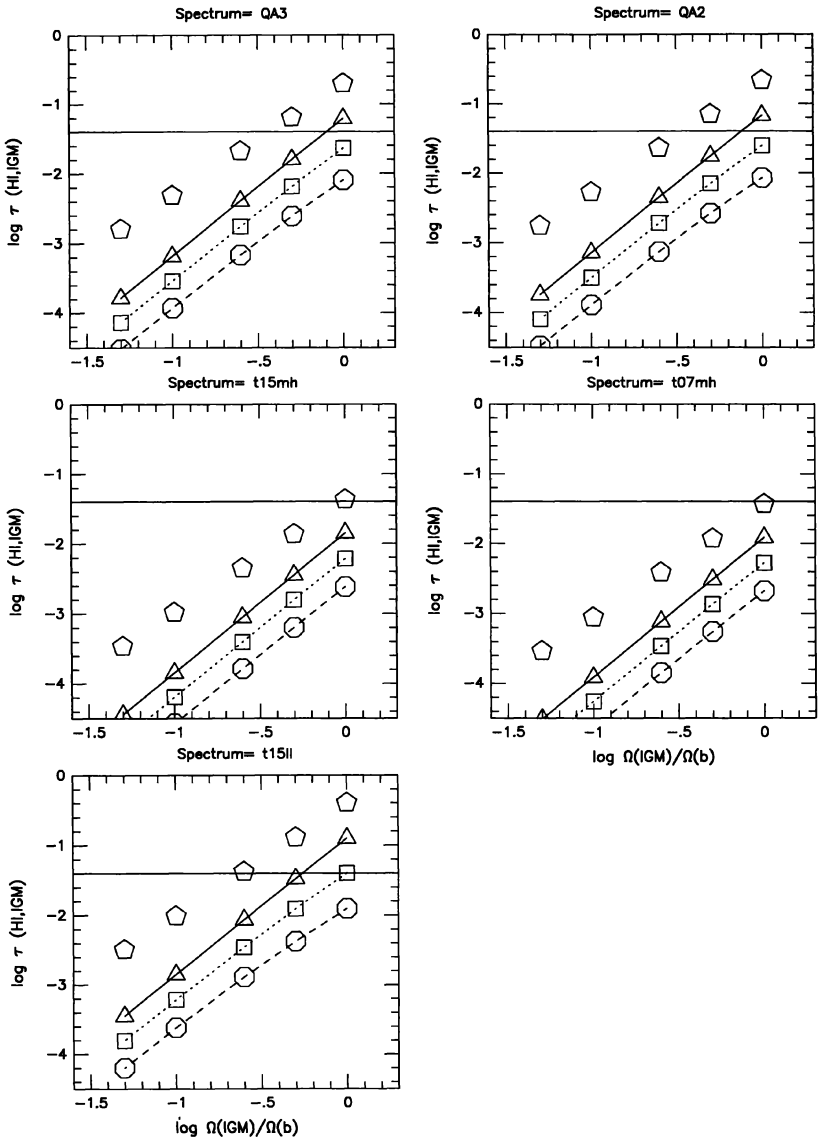

Fig. 7. H I Gunn-Peterson optical depth of the IGM vs. the ratio of $\Omega_{\rm IGM}/\Omega_{\rm b}$. The horizontal line shows the upper limit obtained by Giallongo et al. (1992). In each figure, $T_{\rm IGM}$ is assumed to be 10^5 K (solid line with triangle), 3×10^5 K (dotted line with square), and 10^6 K (dashed line with circle). The open pentagons indicate the IGM in the photoionization and thermal equilibria under the UV background.

depth, there is little information. Since Tripp, Green, and Bechtold (1990) found no detection at $z = 1.722$ in the IUE data, they could only set the 3σ upper limit on $\tau_{\rm He\,I} < 0.21$. We calculated the He I optical depth in order to confirm that our photoionization models predict negligible intervening absorption of He I.

Following the method outlined by Gunn and Peterson (1965), the optical depth due to the IGM, $\tau_{X_i}^{\rm GP}$ (X_i =H I, He I, and He II) is given by

$$\tau_{X_i}^{\rm GP} = \frac{n_{X_i}^{\rm IGM}(z)}{H_0(1+z)(1+2q_0z)^{1/2}}\left(\frac{\pi e^2 f_{X_i}}{m_{\rm e}\nu_{X_i}}\right), \qquad (24)$$

where $H_0 = 100\ h_{100}$ km s^{-1}Mpc^{-1} is the Hubble constant, f_{X_i} is the oscillator strength and ν_{X_i} is the fre-

Table 1. Parameter sets for the promising model* and the He II optical depth.

z_{abs}	$\delta^{\dagger}$	$\zeta^{\ddagger}$	Ω_{IGM}/Ω_b	$\tau^c_{He\,II}$	$\tau^{GP}_{He\,II}$
2.4	$2.0 \le \delta < 2.5$	> 0.5	$0.25 < \Omega_{IGM}/\Omega_b \le 0.5$	$0.5 \lesssim \tau^c_{He\,II} \lesssim 0.7$	$0.06 < \tau^{GP}_{He\,II} \le 0.30$
3.0	$2.0 < \delta \le 2.5$	≥ 0.5	$0.25 \le \Omega_{IGM}/\Omega_b < 0.5$	$1.0 \lesssim \tau^c_{He\,II} \lesssim 1.5$	$0.15 \le \tau^{GP}_{He\,II} < 0.47$

* Both the Lyman α clouds and the IGM are in the photoionization and thermal equilibria under the integrated UV background (model QA2). The resultant $\tau^c_{H\,I}$ and $\tau^{GP}_{H\,I}$ explain the observational limits at the relevant redshifts.

† Power index of the mass function of the Lyman α clouds.

‡ $b_{He\,II}/b_{H\,I}$: the ratio of Doppler parameter between He II line and H I line.

quency of the Lyman α line of each ion. In an $\Omega = 1$ universe with $q_0 = 0.5$, the optical depths of H I, He I, and He II are given by

$$\tau^{GP}_{H\,I} = \frac{4.14 \times 10^{10} h_{100}^{-1} n^{IGM}_{H\,I}(z)}{(1+z)^{3/2}}, \tag{25}$$

$$\tau^{GP}_{He\,II} = \frac{1.32 \times 10^{10} h_{100}^{-1} n^{IGM}_{He\,II}(z)}{(1+z)^{3/2}}, \tag{26}$$

$$\tau^{GP}_{He\,I} = \frac{1.03 \times 10^{10} h_{100}^{-1} n^{IGM}_{He\,I}(z)}{(1+z)^{3/2}}. \tag{27}$$

Hereafter, $h_{100} = 0.7$ is adopted throughout this paper.

We assumed that the hydrogen number density in the IGM is given by

$$n^{IGM}_H(z) = 1.0 \times 10^{-7} \left(\frac{\Omega_{IGM}}{\Omega_b}\right) \left(\frac{\Omega_b}{1.25 \times 10^{-2}}\right) \times \left(\frac{h_{100}}{0.7}\right)^2 (1+z)^3 \mathrm{cm}^{-3}; \tag{28}$$

$$\frac{\Omega_{IGM}}{\Omega_b} = 1,\ 0.5,\ 0.25,\ 0.1,\ 0.05, \tag{29}$$

where the baryon density parameter Ω_b is set as $\Omega_b h_{100}^2 = 1.25 \times 10^{-2}$ (Walker et al. 1991). The critical hydrogen density was defined as $n_{H,crit}(z=0) = 3H_0^2/[8\pi G m_H(1 + 4n_{He}/n_H)] = 8.44 \times 10^{-6} h_{100}^2\,\mathrm{cm}^{-3}$. Note that even if Ω_{IGM}/Ω_b is equal to unity, $n^{IGM}_H(z=0)$ is less than the upper limit on the hydrogen density of the IGM derived by Steidel and Sargent (1987). The helium mass fraction is set as $Y = 0.24$ (which gives $n_{He}/n_H = 0.08$), consistent with the standard primordial nucleosynthesis (Walker et al. 1991). The temperature of the IGM is uncertain, because the IGM probably experienced a reionization epoch and was heated during it. The physical properties in the reionization epoch are still unclear. It was beyond the topic of the present study to investigate them. We then assumed the temperature of the IGM to be $T_{IGM} = 1.0\times10^5$, 3.0×10^5, or 1.0×10^6 K. These ranges of temperature and the amount of the IGM are consistent with the observed y-parameter and the nature of the Lyman α forests (Okoshi, Ikeuchi 1996). In such cases, we solved the photoionization equilibrium at a given T_{IGM}. We also calculated the photoionization models with T_{IGM} derived under the photoionization and thermal equilibria, which gave the lowest case of T_{IGM} ($\lesssim 2 \times 10^4$ K).

The resultant $\tau^{GP}_{H\,I}$ and $\tau^{GP}_{He\,II}$ at $z \simeq 3$ are presented in figures 7 and 9, respectively. Figure 8 shows the visual score of the photoionization models concerning the observational limit on $\tau^{GP}_{H\,I}$ at $z \simeq 3$. All of the results in the redshift range $z = 2.2$–2.6 are smaller than the corresponding results at $z \simeq 3$, within a difference of a factor of 2. When the ionizing background has $I_{\nu_{LL}} = 10^{-21}$erg s^{-1}cm^{-2}Hz^{-1}sr^{-1} (models T15Mh and T07Mh), all such models explain the observed H I opacity, but fail to reproduce the He II opacity. The resultant $\tau_{He\,I}$ is at most several tenths, when $\Omega_{IGM}/\Omega_b \ge 0.5$. On the other hand, the H I Gunn-Peterson test requires $\Omega_{IGM}/\Omega_b < 0.5$, independent of the actual spectral shape, when the UV background has a moderate hydrogen Lyman-limit intensity as $I_{\nu_{LL}} < 10^{-21}$erg s^{-1}cm^{-2}Hz^{-1}sr^{-1}, and the IGM is not hot ($T_{IGM} \lesssim 10^5$K). Such models predict a smaller $\tau_{He\,I}$ than unity. If the amount of the IGM is in the range $0.25 \lesssim \Omega_{IGM}/\Omega_b \lesssim 0.5$, the photoionization models give $\tau^{GP}_{He\,II} \ge 0.1$. Only when the models give a larger $\tau^{GP}_{H\,I}(> 0.1)$ than the 3σ upper limit of the observation, $\tau^{GP}_{He\,II} > 1$ is obtained.

There is no photoionization model that can simultaneously explain the observational limits on both $\tau^{GP}_{H\,I}$ and $\tau^{GP}_{He\,II}$ at the relevant redshifts. However, the photoionized IGM with $0.25 \le \Omega_{IGM}/\Omega_b \lesssim 0.5$ satisfies the observational limit on the H I Gunn-Peterson optical depth, and contributes to the He II opacity at $z \simeq 2$–3 when the UV background has a moderate intensity at the hydrogen Lyman limit, as $I_{\nu_{LL}} \lesssim 10^{-21}$erg s^{-1}cm^{-2}Hz^{-1}sr^{-1}. The summation of the Gunn-Peterson optical depth and the line-blanketing effect of the Lyman α clouds can explain the observational limits on both H I and He II. We present a parameter set for a promising combination of the IGM

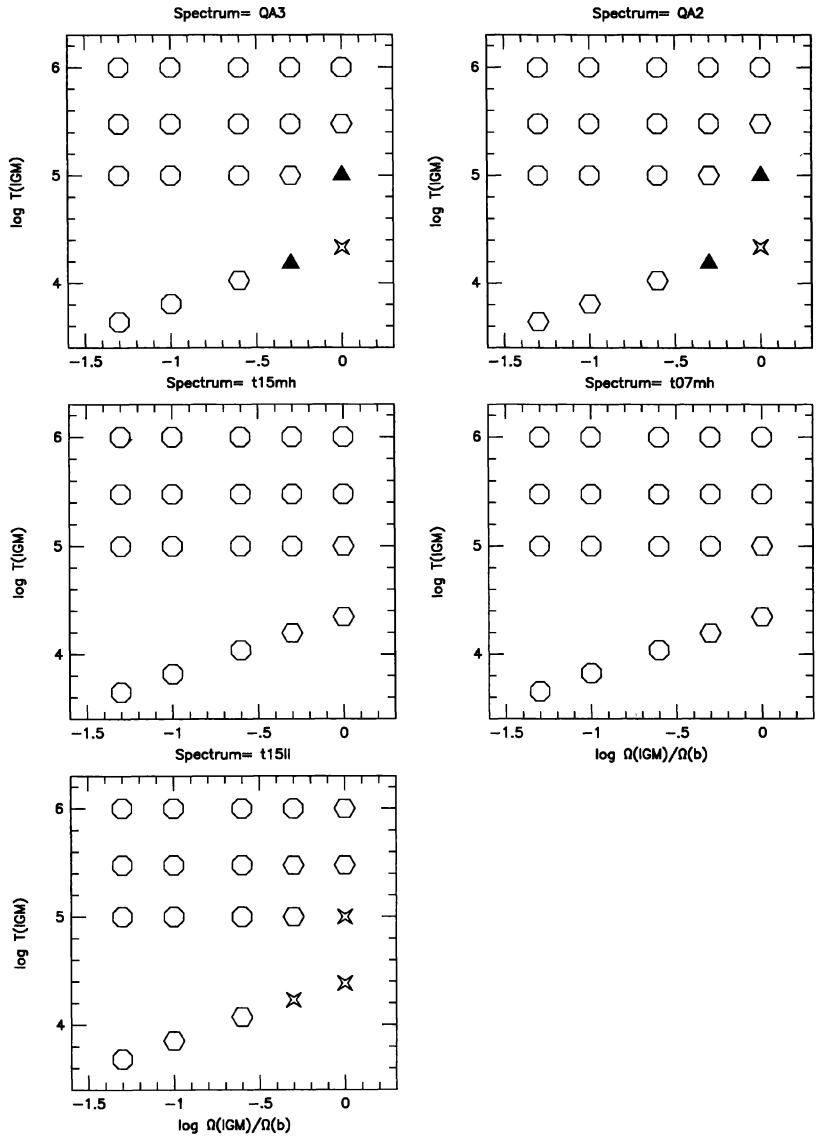

Fig. 8. Visual score of the IGM models, which explain the observational limit on $\tau_{\rm H\,I}^{\rm GP}$. The crosses indicate unsuccessful parameter sets, the filled triangles marginal cases, and the others successful models.

and the Lyman α clouds in table 1. Note that if the temperature of the IGM is sufficiently high ($T_{\rm IGM} > 10^5$ K), the He II absorption due to the IGM would be negligible, even if $\Omega_{\rm IGM} = \Omega_{\rm b}$. This suggests that the IGM was not heated much during the reionization epoch, nor is there any significant energy input (e.g. active star formation and supernova explosions) at $z = 2$–3. The optical depth due to He I in the IGM is negligible in all of the photoionization models, as expected.

5. Conclusions

In this paper we examined the line-blanketing effect due to gaseous clouds at high redshifts. We calculated the ionization states of gas clouds with subgalactic mass scale exposed to an optimum radiation field that can reproduce the ionization states of the Lyman limit systems along the line of sight to quasar HS 1700+6416 (Reimers et al. 1992; Vogel, Reimers 1993, 1995; Reimers, Vogel

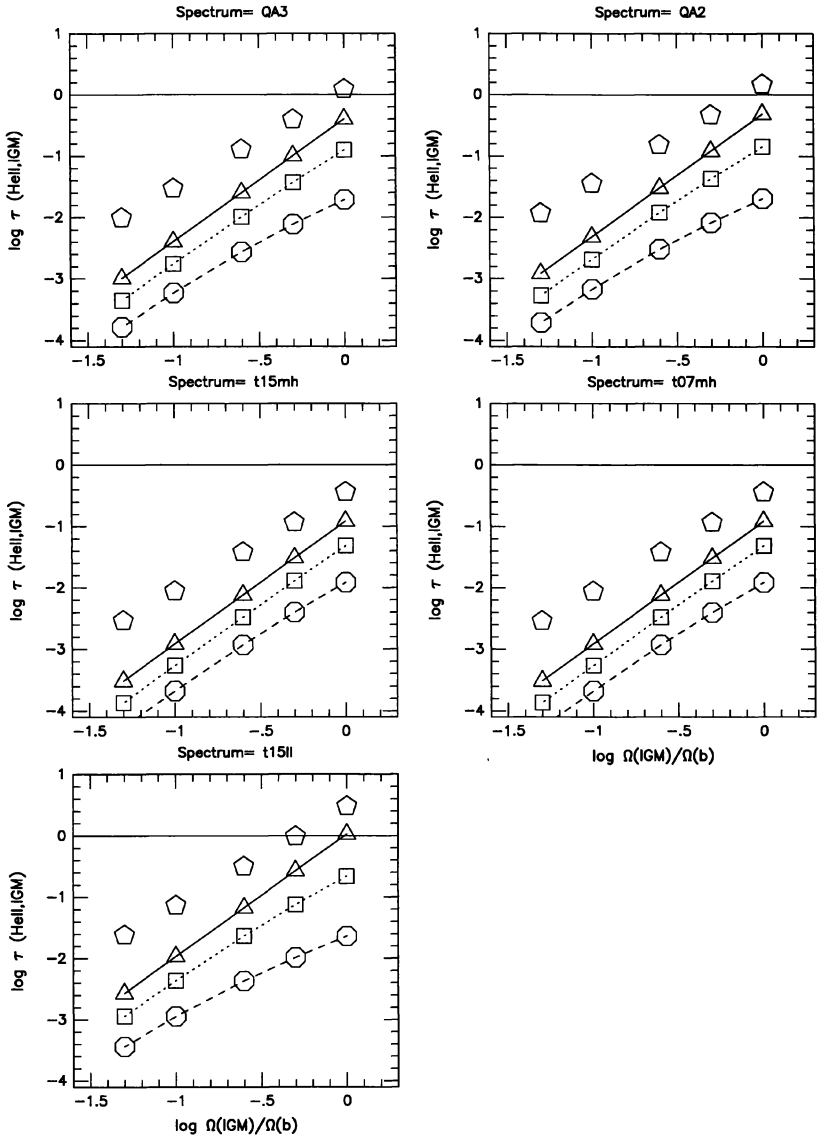

Fig. 9. He II Gunn-Peterson optical depth vs. the ratio of $\Omega_{\rm IGM}/\Omega_{\rm b}$. The horizontal line shows the lower limit. In each figure, $T_{\rm IGM}$ is assumed to be 10^5 K (solid line with triangle), 3×10^5 K (dotted line with square), and 10^6 K (dashed line with circle). The open pentagons indicate the IGM in the photoionization and thermal equilibria under the UV background.

1993). Moreover, the integrated UV radiation from the observed quasars modified by the intervening absorption due to the Lyman α forest and LLSs was adopted as the ionizing spectrum. We calculated the column density distribution of H I, He I, and He II, and finally obtained the line-blanketing optical depths of these ions due to the Lyman α clouds, and the Gunn-Peterson optical depths due to the IGM at $z \simeq 2.2$–3.

A summary of our results is as follows: 1) Our photoionization models with the power index of the mass function $\delta = 1.5$–2 are suitable for the observed $dn/dN_{\rm H\,I}$ in the range of $N_{\rm H\,I} \simeq 2 \times 10^{12}$–$10^{15}{\rm cm}^{-2}$. However, the mass function with $2 \lesssim \delta \lesssim 2.5$ is still consistent with the observation. 2) The integrated UV background models explain the observed ratio of C IV/H I better than the optimum broken power-law models. The shape of

the ionizing radiation is probably more important than the metallicity to explain the observed C IV/H I ratio of the Lyman α clouds. 3) The line-blanketing effect of the Lyman α clouds following the mass function with $\delta = 2.0$ can reproduce the observed $\tau^{c}_{\rm H\,I}$ at $\langle z \rangle = 2.4$, but not $\tau^{c}_{\rm He\,II}$. The resultant $\tau^{c}_{\rm He\,II}$ is smaller than 0.7, even if the He II absorption line is broadened due to turbulence. On the other hand, the Lyman α clouds with $\delta \simeq 2.5$ can reproduce both $\tau^{c}_{\rm H\,I}$ and $\tau^{c}_{\rm He\,II}$ at $z \sim 3$ simultaneously. If the He II optical depth is larger than 1.5 at $z \sim 3$, these clouds would fail to explain the observation. 4) If the real He II optical depth is larger than 3 at $z \sim 3$, none of the photoionization models considered here can explain such a large $\tau_{\rm He\,II}$. Any other source of opacity, such as substantial diffuse IGM, very weak Lyman α clouds with $N_{\rm H\,I} < 10^{12}{\rm cm}^{-2}$, or both are therefore necessary. 5) The IGM probably contributes to the He II optical depth, and safely explains the H I Gunn-Peterson optical depth, simultaneously. The amount of the IGM and temperature are required to be $0.25 \leq \Omega_{\rm IGM}/\Omega_{\rm b} \lesssim 0.5$ and $T_{\rm IGM} \lesssim 10^5$ K. The UV background has a moderate hydrogen Lyman-limit intensity as $I_{\nu_{\rm LL}} \lesssim 10^{-21}{\rm erg\ s^{-1}cm^{-2}Hz^{-1}sr^{-1}}$.

The integrated UV background radiation of quasars can well explain the ionization states of both the IGM and the Lyman α clouds at $z \sim 2$–3. Both the IGM and the Lyman α clouds may be in the photoionization and thermal equilibria under such UV background radiation. At most half of the dark baryons consists of the IGM ($0.25 \leq \Omega_{\rm IGM}/\Omega_{\rm b} \lesssim 0.5$). The mass function of the Lyman α clouds follows a power law, $dn/dM_{\rm c} \propto M_{\rm c}^{-\delta}$ with $\delta \sim 2$–2.5 in the 10^8–$10^{11} M_\odot$ range. The UV background radiation probably has a flat spectrum in the $\sim$ 13.6–54.4 eV energy band, and a break at the He II edge rather than a steep spectrum in the relevant energy band. Quasars are a promising source of the UV background.

The authors thank the referee, Prof. P. Madau, for his valuable comments, from which the manuscript benefited.

References

Allen C.W. 1973, Astrophysical Quantities, 3rd ed (Athlone Press, London) p31

Bahcall J.N., Bergeron J., Boksenberg A., Hartig G.F., Jannuzi B.T., Kirhakos S., Sargent W.L.W., Savage B.D. et al. 1996, ApJ 457, 19

Bechtold J. 1988, in High Redshift and Primeval Galaxies, ed J. Bergeron, D. Kunth, B. Rocca-Volmerange, J. Tran Thanh Van (Editions Frontières, Gif-sur-Yvette) p397

Bechtold J. 1994, ApJS 91, 1

Bechtold J., Weymann R.J., Lin Z., Malkan M.A. 1987, ApJ 315, 180

Boyle B.J. 1991, in Proc. 1990 Texas/ESO-CERN Symp. on Relativistic Astrophysics (Academy of Sciences, New York) p14

Carswell R.F., Lanzetta K.M., Parnell H.C., Webb J.K. 1991, ApJ 371, 36

Chernomordik V.V. 1995, ApJ 440, 431

Cowie L.L., Songaila A., Kim T.-S., Hu E.M. 1995, AJ 109, 1522

Cristiani S., D'Odorico S., Fontana A., Giallongo E., Savaglio S. 1995, MN 273, 1016

Crotts A.P.S. 1989, ApJ 336, 550

Davidsen A.F., Kriss G.A., Zheng W. 1996, Nature 380, 47

Denda K., Ikeuchi S. 1993, PASJ 45, L1

Denda K., Ikeuchi S. 1995, PASJ 47, 877 (Paper I)

Giallongo E., Cristiani S., Trevese D. 1992, ApJ 398, L9

Giroux M.L., Fardal M.A., Shull J.M. 1995, ApJ 451, 477

Giroux M.L., Sutherland R.S., Shull J.M. 1994, ApJ 435, L97

Gunn J.E., Peterson B.A. 1965, ApJ 142, 1633

Hu E.M., Kim T.-S., Cowie L.L., Songaila A., Rauch M. 1995, AJ 110, 1526

Ikeuchi S., Murakami I., Rees M.J. 1989, PASJ 41, 1095

Jakobsen P., Boksenberg J.M., Deharveng J.M., Greenfield P., Jedrzejewski R., Paresce F. 1994, Nature 370, 35

Jenkins E.B., Ostriker J.P. 1991, ApJ 376, 33

Lanzetta K.M. 1991, ApJ 375, 1

Lu L. 1991, ApJ 379, 99

Madau P. 1992, ApJ 389, L1

Madau P., Meiksin A. 1994, ApJ 433, L53

Meiksin A., Madau P. 1993, ApJ 412, 34

Miralda-Escudé J. 1993, MN 262, 273

Miralda-Escudé J., Ostriker J.P., 1990, ApJ 350, 1 (MO90)

Miralda-Escudé J., Ostriker J.P., 1992, ApJ 392, 15

Miralda-Escudé J., Rees M.J. 1994, MN 266, 343

Morris S.L., Weymann R.J., Dressler A., McCarthy P.J., Smith B.A., Terrile R.J., Giovanelli R., Irwin M. 1993, ApJ 419, 524

Murakami I., Ikeuchi S. 1993, ApJ 409, 42

Norris J., Hartwick F.D., Peterson B.A. 1983, ApJ 273, 450

O'Brien P.T., Gondhalekar P.M., Wilson R. 1988, MN 233, 801

Oke J.B., Korycansky D.G. 1982, ApJ 255, 11

Okoshi K., Ikeuchi S. 1996, PASJ 48, 441

Paresce F., McKee C., Bowyer S. 1980, ApJ 240, 387

Petitjean P., Webb J.K., Rauch M., Carswell R.F., Lanzetta K.M. 1993, MN 262, 499

Rees M.J. 1988, in QSO Absorption Lines: Probing the Universe, ed J.C. Blades, D.A. Turnshek, C.A. Norman (Cambridge University Press, Cambridge) p107

Reimers D., Vogel S. 1993, A&A 276, L13

Reimers D., Vogel S., Hagen H.-J., Engels D., Groote D., Wamsteker W., Clavel J., Rosa M.P. 1992, Nature 360, 561

Sargent W.L.W., Steidel C.C., Boksenberg A. 1989, ApJS 69, 703

Sargent W.L.W., Young P.J., Boksenberg A., Tytler D. 1980, ApJS 42, 41

Schneider D.P., Schmidt M., Gunn J.E. 1991, AJ 101, 2004

Songaila A., Hu E.M., Cowie L.L. 1995, Nature 375, 124

Steidel C.C., Sargent W.L.W. 1987, ApJ 318, L11

Stengler-Larrea E.A., Boksenberg A., Steidel C.C., Sargent W.L.W., Bahcall J.N., Bergeron J., Hartig G.F., Jannuzi B.T. et al. 1995, ApJ 444, 64
Tripp T.M., Green R.F., Bechtold J. 1990, ApJ 364, L29
Tytler D. 1987, ApJ 321, 49
Tytler D., Fan X.-M., Burles S., Cottrell L., Davis C., Kirkman D., Zuo L. 1995, in QSO Absorption Lines, Proc. ESO Workshop, ed J. Bergeron, G. Meyland, J. Wampler (Springer, Heidelberg) p289
Vogel S., Reimers D. 1993, A&A 274, L5
Vogel S., Reimers D. 1995, A&A 294, 377
Walker T.P., Steigman G., Kang H.-S., Schramm D.M., Olive K.A. 1991, ApJ 376, 51
Webb J.K., Barcons X., Carswell R.F., Parnell H.C. 1992, MN 255, 319
Zamorani G., Maccacaro T., Henry J.P., Tananbaum H., Soltan A., Liebert J., Stocke J., Strittmatter P.A. et al. 1981, ApJ 245, 357